Green Chemistry

PAPER

View Article Online
View Journal

Cite this: DOI: 10.1039/d5gc06304c

Cascading integration of genetically reduced cellulose nanofibers and ultrasound-dissected fungi mycelium for the synergistic enhancement of cellulases and saccharification with high-value bioproducts

Hao Peng,†[a,b,c] Peng Liu,†[a] Jingyuan Liu,[a,b] Junsheng Yu,[a] Boyang He,[a,c] Yujing Yang,[a] Hua Yu,[a] Heng Kang,[a] Mengzhou Zhou,[a] Wanbin Zhu,[d] Muhammad Nauman Aftab,[e] Yanting Wang,*[a] Chunxiang Fu*[b] and Liangcai Peng*[a,c]

Plants provide enormous convertible biomass resources for biofuels and bioproducts, but the recalcitrant nature of lignocellulose presents a critical difficulty in achieving optimal enzyme complexes that are universally capable of diverse biomass saccharification. In this study, lignocellulose-degradation enzymes were obtained with high activity and high yield by the application of optimized ultrasound treatment for two distinct fungi (*T. reesei* and *A. niger*) incubations with desired rice mutant straws. The approach enabled a characteristically synergistic enhancement for biomass saccharification of three representative bioenergy plants (eucalyptus, fern, and rice), with yields of hexoses increased up to 7.7 folds. All retained residues of digested lignocelluloses and dissected mycelium were directly used as active biosorbents for Congo red (CR) and methylene blue (MB), with adsorptions of 165.6 mg g^{-1} and 184.8 mg g^{-1}, respectively. They could also be converted into highly porous biocarbon materials with further upgraded dye adsorptions of 2766.3 mg g^{-1} (CR) and 491.5 mg g^{-1} (MB) and with a 2-fold improved specific capacitance. A mechanism model is thus proposed to illustrate how the integration of genetically engineerable plant lignocelluloses with ultrasound-dissectible fungi mycelium can enhance cellulase secretion and biomass saccharification, thereby contributing to a sustainable bioeconomy through green-like biomass processes.

Received 24th November 2025,
Accepted 11th February 2026

DOI: 10.1039/d5gc06304c

rsc.li/greenchem

Green foundation

1. This study integrated four typically green-like technologies: (1) length-reduced cellulose nanofibrils were generated from a natural rice mutant; (2) optimal ultrasound treatment was performed for two distinct fungi incubations with mutant substrates; (3) optimal incorporation of two fungal-secreted enzymes was explored for synergistically enhanced biomass saccharification; and (4) all remaining lignocelluloses and mycelium were examined as advanced desirable biosorbents and highly porous biocarbon with increased dye adsorption and electrochemical conductivity.
2. Cascading integration of four green-like processes could efficiently produce lignocellulose-degradation enzymes that upgraded sugar yield by 7.7 folds, dye adsorption by 4–17 folds, and electrochemical conductivity by 2 folds.
3. A novel green-like strategy is proposed for cascading biomass conversion as part of a sustainable bioeconomy. Ultrasound can be simply applied for the simultaneous modification of plant lignocelluloses and fungal mycelium as a green-integrated chemistry approach for improving biofuel and multiple-bioproduct generation in the field.

[a]*Key Laboratory of Fermentation Engineering (Ministry of Education), National "111" Center for Cellular Regulation & Molecular Pharmaceutics, Cooperative Innovation Center of Industrial Fermentation (Ministry of Education & Hubei Province), Hubei Key Laboratory of Industrial Microbiology, Biomass & Bioenergy Research Center, School of Life & Health Sciences, Hubei University of Technology, Wuhan, 430068, China. E-mail: lpeng@mail.hzau.edu.cn, wyt@mail.hzau.edu.cn; https://bbrc.hbut.edu.cn*

[b]*Shandong Provincial Key Laboratory of Energy Genetics, CAS Key Laboratory of Biofuels, Qingdao Institute of Bioenergy & Bioprocess Technology, Chinese Academy of Sciences; Shandong Energy Institute; Qingdao New Energy Shandong Laboratory, Qingdao 266101, China. E-mail: fucx@qibebt.ac.cn*

[c]*College of Plant Science & Technology, Huazhong Agricultural University, Wuhan 430070, China*

[d]*Center of Biomass Engineering, College of Agronomy & Biotechnology, China Agricultural University, Beijing 100193, China*

[e]*Institute of Industrial Biotechnology, Govt. College University, Lahore 54000, Pakistan*

† The authors contributed equally.

1. Introduction

During biological evolution, plant photosynthesis signifies a unique carbon fixation pathway for the production of edible carbohydrates and convertible lignocelluloses, whereas fungi survive on carbohydrates by digesting lignocelluloses as carbon sources.[1,2] Although plant cell walls provide enormous amounts of lignocelluloses that can be converted into biofuels and bioproducts, their natural recalcitrance invariably requires costly biomass processing along with secondary waste release into the environment.[3–6] As biomass enzymatic saccharification is a crucial step for biomass processing, it thus becomes essential to explore the production of lignocellulose-degradation enzymes that are relatively low-cost and exhibit high efficiency.[7–9]

As a common fungal strain, *Trichoderma reesei* (*T. reesei*) is extensively employed for the production of cellulase complexes such as exoglucanases (CBHs), endoglucanases (EGs), β-glucosidases (BGs), and xylanases, which are involved in the distinct catalysis of lignocellulose hydrolysis into fermentable hexoses and pentoses.[10–12] However, *Aspergillus niger* (*A. niger*) is a specific fungal strain that secretes lignocellulose-degradation enzymes, particularly BGs, with remarkably high activities.[13–15] Over the past years, genetic engineering of fungal strains has been broadly implemented to improve enzyme production, but it remains a biotechnological difficulty to produce optimal cellulase complexes that are universally applicable for efficient hydrolysis of different lignocellulose substrates from diverse plant species.[11,16] Alternatively, advanced technology is being used to enhance fungal secretions by introducing active inducers and various carbon sources.[17,18] For example, length-reduced cellulose nanofibers (CNFs) from a natural rice site-mutant (*Osfc16*) are utilized as a carbon source for incubation with *Trichoderma* for the secretion of high-activity cellulases, enabling consistently enhanced biomass enzymatic saccharification of different bioenergy crops.[19] Likewise, rice site-mutants have recently been obtained using clustered regularly interspaced short palindromic repeats/associated protein 9 (CRISPR/Cas9) technology, and their CNFs are also examined as active carbon sources for improved *Trichoderma reesei* secretion of high-activity cellulase complexes in high yields.[20] Importantly, the assembly of CNFs, as characterized by the density of amorphous cellulose chains, is identified as a key factor that negatively correlates with lignocellulose recalcitrance in plants. This finding provides an important insight for universally enhancing fungal secretion of lignocellulose-degrading enzymes.[9,21]

As a green and sustainable technology, ultrasound treatment is increasingly being applied in agriculture, industry, energy and medical fields, because it provides multiple advantages such as high activation energy for complete mass penetration and short processing times for simple operation.[22,23] Recently, ultrasound pretreatment has been used for the effective deconstruction of lignocelluloses by selectively removing hemicellulose and lignin, enhancing cellulose surface accessibility and facilitating the penetration of cellulases for biomass saccharification.[24–27] Hence, it remains interesting to explore the potential role of ultrasound treatment in fungal incubation with lignocellulose substrate for promoting the secretion of biomass-degradation enzymes.

In this study, the natural rice mutant (*Osfc16*) was replanted to collect mature straw as a carbon source for fungal incubation (Fig. S1). By using well-established methods, two fungi strains (*T. reesei* and *A. niger*) were respectively incubated with the mutant lignocelluloses to secrete lignocellulose-degradation enzymes, and ultrasound treatment under various conditions was performed during fungal co-cultivation. By establishing the optimal ultrasound treatment, this study enabled distinctly improved activities and yields of cellulase complexes secreted from the two fungi strains. Further, by incorporating the two fungi-secreted enzymes in optimal proportions, this study determined a synergistically enhanced biomass enzymatic saccharification. Notably, this work established how the optimal ultrasound treatment could dissect fungal mycelium for active interaction with reduced lignocelluloses to universally enhance fungal secretion of cellulases with high yields and high activities. After fungal incubation, the dimension-minimized nano-lignocellulose residues and dissected fungal mycelium were used directly as desirable biosorbents with high adsorption of two distinct industrial dyes. The desirable biosorbents were further employed to generate a highly porous biocarbon material that exhibits exceptionally high dye adsorption and superior electrochemical performance. Therefore, this study demonstrates an integrative biotechnology of plants and fungi as a novel strategy for improved synergistic production of cellulases and sugars, along with the exceptional benefits of bioproduction. Collectively, this work demonstrates that the integration of rice site-mutant straw containing high-density CNFs and two fungi incubations under optimal ultrasound treatment could clearly improve the secretion of complementary lignocellulose-degradation enzymes, thereby enabling synergistically enhanced biomass saccharification and valorizing homogeneous residues for high-performance biosorbents and biocarbon materials for use in a sustainable bioeconomy.

2. Materials and methods

2.1. Biomass and enzyme collection

Mature straw from the rice mutant (*Osfc16*; *Oryza sativa* L.) and wild type (WT; Nipponbare) were cultivated at the experimental field of Huazhong Agricultural University in Wuhan, China. Stem tissues of the rice mutant (*Osfc16*; *Oryza sativa* L.) and wild type (WT; Nipponbare) were desiccated at a temperature of 55 °C and subsequently fragmented into small segments, pulverized through a screen, and preserved in a dry receptacle. Three biomass samples derived from three plants (fern, eucalyptus and rice) were utilized as the substrates for biomass saccharification. Four types of standard enzymes (endoglucanases, exoglucanases, β-glucosidases, and xyla-

nases) were purchased from Megazyme company, and a commercial mixed-enzyme (HSB) was sourced from Imperial Jade Biotechnology Co., Ltd, Ningxia, China.

2.2. Wall polymer extraction and detection

The fractionation of plant cell walls was conducted as previously described.[28] Cellulose was measured by the anthrone/H_2SO_4 method, and the arabinose (Ara) and xylose (Xyl) assays of total hemicellulose were conducted with detection by gas chromatography-mass spectrometry (GC-MS, Shimadzu GCMS-QP2010Plus).[29] Total lignin content was determined through two-step acid hydrolysis.[6] The viscosity method was employed to detect the degree of polymerization (DP) of cellulose, and X-ray diffraction was used to determine the crystalline index (CrI) of cellulose. The DP and CrI values were calculated according to the equations: $DP_{0.905} = 0.75[\eta]$ and $CrI = 100 \times (I_{200} - I_{am})/I_{200}$, as previously described.[20]

2.3. Cellulose nanofibril extraction and observation

NaOH and NaClO were employed for the extraction of crude cellulose, as previously described.[19] Crude cellulose was decomposed to produce cellulose nanofibrils (CNFs) by using a blender (Ultra Turrax T18, IKA, Germany) and a homogenizer (HPH) (AH-1500, ATS, Canada) subjected to homogenization at 60 MPa for 30 cycles. Atomic force microscopy (AFM, MultiMode8, Bruker, USA) was used to observe the CNFs' morphology at a scanning rate of 1 Hz. Gwyddion software (version 2.56) was used for the statistical calculations; 50 randomly selected data points were collected in approximately 10 areas.[9]

2.4. Fungal strain cultivation with rice straw under ultrasound treatment

T. reesei strain (Rut-C30; CICC 40348) was cultivated on potato dextrose agar at 28 °C for 7 days. Fungal conidia were rinsed with double-distilled water (ddH_2O) and measured with a haemocytometer. About 500 μL of suspension, including 6×10^6 spores per milliliter, was incubated with 0.6 g rice straw.[1] The 2% (w/v) solids were loaded into 30 mL of a defined Mandels' medium (pH 4.8) and cultivated in 250 mL Erlenmeyer flasks under agitation at 200 rpm and 28 °C for 7 days to ensure sufficient oxygen transfer. The medium contains 1.4 g L^{-1} $(NH_4)_2SO_4$, 2 g L^{-1} KH_2PO_4, 0.3 g L^{-1} $MgSO_4$, 0.4 g L^{-1} $CaCl_2$, 0.3 g L^{-1} urea, 1 g L^{-1} peptone, 20 g L^{-1} carbon source, 20 mL L^{-1} trace elements (7.5 mg L^{-1} $FeSO_4 \cdot 7H_2O$, 2 mg L^{-1} $MnSO_4 \cdot H_2O$, 2 mg L^{-1} $ZnSO_4 \cdot H_2O$ and 3 mg L^{-1} $CoCl_2 \cdot 2H_2O$). During the 7-day cultivation, ultrasound treatment was employed using an ultrasonic processor (SB-3200DTD, China) operating at a power of 72, 108, and 144 W for 1, 2, and 4 minutes. The ultrasound treatment was also conducted on the 3rd day (repeated 1 time), 2nd, 4th, and 6th day (repeated 3 times) and daily (repeated 6 times) during the *T. reesei* incubation period. *A. niger* strain (1956S) was collected with Tween-80, and the fungal incubation with rice straw was conducted at 30 °C for 7 days as described for the *T. reesei* strain above. Ultrasound treatment was employed at 108, 144, 180 W power for 1, 2, 4 min on the 3rd day (repeated 1 time), 2nd, 4th and 6th day (3 times repeating) and every day (6 times repeating) during the 7-day *A. niger* strain (1956S) incubation. The crude cellulase solutions from the fungal secretions were collected for assays of lignocellulose-degradation enzyme activities and total protein levels.

2.5. Filter paper activity and protein assay

Filter paper activity (FPA) and protein assay were performed as previously described.[30] About 50 mg of Whatman No.1 filter paper was incubated with the fungal-secreted crude enzymes at 50 °C for 1 h, followed by 2 mL DNS boiling for 10 min. Coomassie Brilliant Blue G250 was utilized for protein content determination as previously described.[31] Sodium dodecyl sulfate-polyacrylamide gel electrophoresis (SDS-PAGE) was run to separate proteins secreted by fungal incubation, and the major enzymes were identified by liquid chromatography-tandem mass spectrometry (LC-MS/MS, Jingjie PTM BioLab Co., Ltd, Hangzhou, China; Orbitrap Elite LC-MS/MS, Thermo, USA) as previously described.[19]

2.6. Enzyme activity assay *in vitro*

The activities of endoglucanase, exoglucanase, β-glucosidase and xylanase were respectively determined by using substrates including carboxymethyl cellulose sodium salt (CMC-Na), *p*-nitrophenyl β-D-cellobioside (*p*NPC), salicin, and beechwood xylan, as previously described.[1,17] The enzymes were inactivated at 100 °C for 10 minutes as experimental controls. One unit of enzyme activity (*U*) was defined by the release of 1 μmol glucose/xylose per minute. All enzyme assays were accomplished as independent triplicates.

2.7. Characterization of fungal incubations with rice straw under ultrasound treatment

The supernatants were collected from fungal incubations, and the hexoses and pentoses of the supernatants were determined by the anthrone/H_2SO_4 and chloride/HCl methods, respectively. The protein levels of the supernatants were measured as described above.[31] A surface/interface tensiometer (K100, America) was used to detect the interfacial tension of supernatants collected from fungal incubation for 7 days. The test commenced once the plate was brought into proximity to the liquid level of the beaker with the supernatants. After the measurement was completed, the plate was subjected to a burning process for 3–5 minutes.

The lignocellulose residues were observed under AFM, as previously described,[9] and the residues were photographed with 512 × 512 pixels. Fourier-transform infrared (FT-IR) spectroscopy was used to determine the chemical properties of lignocellulose residues, as previously described.[32] Fungal growths and lignocellulose digestion were observed with Image View software through fluorescence microscopy (Yongxin NE910, China) during incubation with the rice straw under optimal ultrasound treatment. Fungal strains were labeled under fluorescence with trypan blue, and the rice straw was stained with Calcofluor under microscopy.

2.8. Biomass pretreatment and enzymatic hydrolysis

Alkali pretreatments of three bioenergy crops (fern, eucalyptus, rice) were conducted with 0.5% NaOH (w/v) at 50 °C for 2 h under 150 rpm shaking, as previously described.[20] After centrifugation at 3000*g* for 5 min, the solid residues were subjected to enzymatic hydrolysis using a solution of cellulases secreted by the fungal incubations or commercial mixed-cellulases (HSB, 10 FPU g^{-1}) at 50 °C under 150 rpm shaking for 2 days. The 1.25% (w/v) solid residues were loaded into 8 mL of 50 mM sodium phosphate buffer (pH 4.8). For a standard comparison, all enzymatic hydrolysis experiments were conducted at a matched filter paper activity (FPA) loading of 10 FPU per gram of enzyme preparation. The FPA of each enzyme preparation (fungal supernatants and commercial HSB) was determined by following the standard method, and the volumes used were adjusted for comparison of saccharification efficiency. After enzymatic hydrolysis, the hexoses and pentoses of the supernatants were measured as previously described.[1,11] All assays were accomplished as independent triplicates.

2.9. Biocarbon generation and characterization

The lignocellulose residues after *T. reesei* incubation under ultrasound treatment were thoroughly mixed with $FeCl_2{\cdot}4H_2O$ in a 1 : 2 ratio (w/w) and subsequently pulverized into powders. The powder mixture was placed in a tubular furnace and heated gradually under a nitrogen atmosphere at a rate of 5 °C per minute to 1000 °C and held at this temperature for 2 hours. After cooling the materials to 300 °C at a rate of 10 °C per minute and subsequently to room temperature, it was soaked in 1 mol L^{-1} HCl for 6–12 h in order to remove other ions. The samples were mixed with ddH_2O until reaching pH 7.0, then treated with ethanol for 2–4 hours in an ultrasonic cleaning machine and dried at 60 °C for 12 hours.[33]

The biocarbon sample was observed under scanning electron microscopy (GeminiSEM 300, ZEISS, Germany) to analyze the surface topography and pore architecture. Nitrogen adsorption/desorption isotherm (BET) assays were conducted using established protocols with a Porosity Analyzer and Automated Surface Area instrument as previously described.[29] X-ray diffraction (XRD) and Raman spectra (Alpha300R, WITec, Germany) were detected with a 2θ range of 10°-80° and a wavenumber range of 500–3500 cm^{-1}, respectively. For composition and binding energy measurements, the biocarbon sample was scanned by X-ray photoelectron spectroscopy (XPS, K-Alpha, Thermo Scientific, USA) as described previously.[34]

2.10. Dye (MB, CR) adsorption assay

About 20 mg biocarbon and lignocellulose residue samples were respectively mixed with 20 mL of dye solutions of MB and CR at room temperature with agitation for 5–8 h, as previously described.[6,33] Samples underwent centrifugation, and the residual dye concentrations in the supernatants were quantified *via* UV-Vis spectrophotometry at 668 nm (MB) and 498 nm (CR). The gradient concentrations of MB and CR solutions were 0.2, 0.3, 0.4, 0.5, 0.6 g L^{-1} and 0.5, 1, 2, 3, 4 g L^{-1}, respectively.

2.11. Electrochemical properties analysis

Electrochemical measurements were conducted with a CHI660E electrochemical workstation at room temperature in 6 M KOH electrolyte, as previously described.[1] Biocarbon, Super-P, and PTFE were combined in an 8 : 1 : 1 weight ratio and ground with ethanol as a dispersing agent. The electrode was fabricated by pressing the aforementioned composite mixture onto nickel foam, with the active material constituting 80% of the total mass. The electrochemical properties of the samples were determined with cyclic voltammetry (CV) and galvanostatic charge–discharge (GCD) tests. The specific capacitance was derived at different current densities (0.5, 5, 10, 15, 20 A g^{-1}), as previously described.[33]

2.12. Statistical analysis

Data analyses were accomplished using a Superior Performance Software System. Statistically significant differences were measured using Student's *t*-test (**p < 0.01, *p < 0.05) and ANOVA for multiple comparisons.

3. Results and discussion

3.1. Distinctly improved cellulase secretions from fungal incubations with rice mutant straw under ultrasound treatment

As ultrasound treatment could reduce the natural lignocellulose recalcitrance to increase cellulose accessibility,[27,35] this study initially employed ultrasound treatment for the classic fungal strain (*T. reesei*) incubation with common rice wild type (WT) straw (Fig. S1 and S2). To establish the optimal ultrasound treatment for enhancing *T. reesei* secretion of lignocellulose-degradation enzymes, various ultrasound conditions were assayed, including ultrasound power (W), treatment time (min) and number of repeats (t). By assessing filter paper activities (FPAs) of the *T. reesei*-secreted solutions, this study determined the optimal ultrasound treatment to be 108 W power for 4 min course under 1 time repeating (108 W, 4 min, 1 t). As a result, the optimal ultrasound treatment achieved significantly higher FPAs and protein contents than those of the controls (without ultrasound) by 58% and 69%, respectively (Fig. S3). Meanwhile, other ultrasound treatments also caused significantly increased FPAs and protein levels at p < 0.05 and 0.01 levels (n = 3). As FPAs are the general parameter accounting for lignocellulose hydrolytic activity,[1,19] the results revealed that ultrasound treatment consistently improved *T. reesei* incubation with rice straw for secretion of lignocellulose-degradation enzymes. In addition, the optimal ultrasound treatment was conducted separately with either the *T. reesei* strain or rice straw before fungal incubation; those two individual treatments did not show any significantly altered FPA or protein levels compared to the control samples (Fig. S4), suggesting that the optimal ultrasound treatment mainly facilitated fungal interaction with lignocellulose substrate to improve enzyme secretion. On the other hand, the results also indicated that the optimal ultrasound treatment with the *T. reesei*

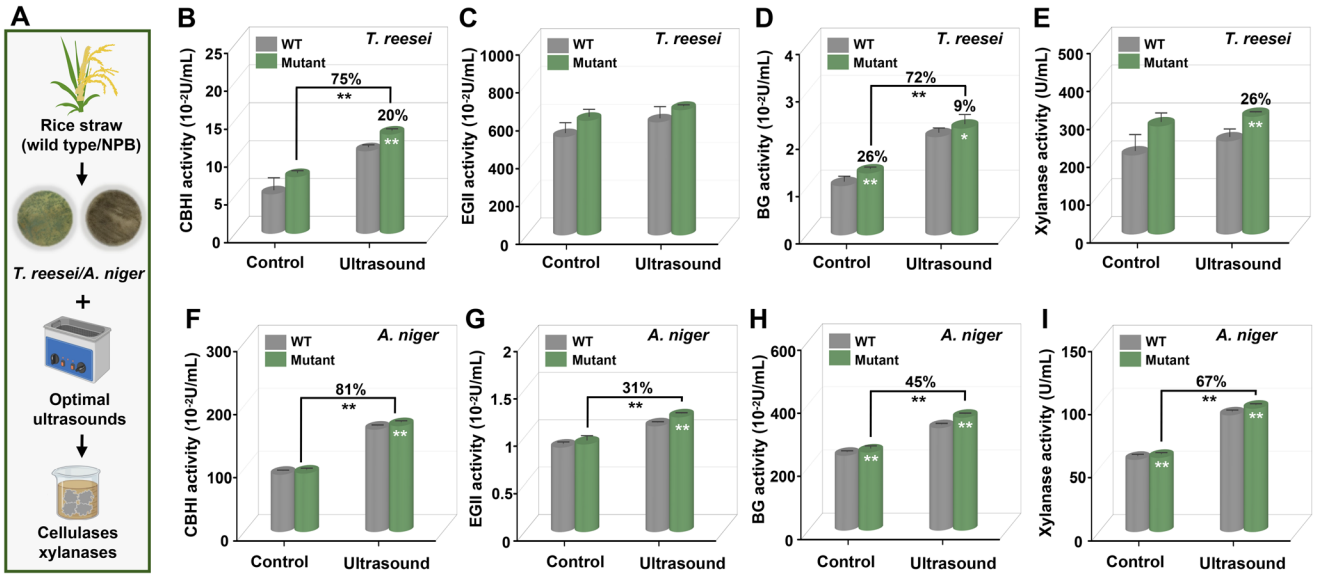

Fig. 1 Dual-enhanced cellulases and xylanases secreted by *T. reesei* and *A. niger* incubations with the desirable rice mutant (*Osfc16*) straw under optimal ultrasound treatment: (A) general procedure for *T. reesei* and *A. niger* incubation for enzymes secretion; (B–E) assay of CBHI, EGII BG and xylanase activities *in vitro* using *T. reesei*-secreted solution; (F–I) enzyme activity assays *in vitro* using *A. niger*-secreted solution. * and ** indicate significant differences at $p < 0.05$ and $p < 0.01$ levels, respectively ($n = 3$). Data are presented as means ± SD. WT: wild type of rice mutant; Control: fungal incubation without ultrasound treatment.

strain did not affect fungal growth for enzyme secretion. Furthermore, this study re-collected the previously-identified rice site mutant (*Osfc16*) to incubate with *T. reesei* under the optimal ultrasound treatment (Fig. 1A). Because the rice mutant consistently showed length-reduced cellulose nanofibril assembly and relatively reduced cellulose levels and features (CrI, DP) accounting for improved lignocellulose recalcitrance (Fig. S5),[36] this study examined significantly raised activities of three major enzymes (CBHI, BG, xylanase) secreted from *T. reesei* incubation with rice mutant, compared to its WT (Fig. 1B–E). In particular, the optimal ultrasound treatment could further increase the activities of two enzymes (CBHI, BG) by 75% and 72%, compared to the control (without ultrasound). However, EGII activities were not significantly altered by the optimal ultrasound treatments in either mutant or WT samples (Fig. 1C). This is likely because *T. reesei* inherently secretes EGII at high levels even without ultrasound treatment.[37,38] Moreover, all major types of enzymes were identified by LC-MS/MS assay of the secreted solution from *T. reesei* incubation with mutant straw, such as two cellobiohydrolases, two *endo*-β-1,4-glucanases, two β-glucosidases, *endo*-1,4-β-xylanase, xyloglucanase and swollenin, revealing that comprehensive cellulase complexes were secreted from fungal incubation (Fig. 2 and Table S1).

Because the *T. reesei* strain could not secrete high-activity CBHI and BG enzymes, ultrasound treatment was performed with another fungal strain (*A. niger*) incubation, which enables secretion of notably higher-activity BGs and CBHIs.[39–41] By establishing the optimal ultrasound conditions at 144 W for 4 min course under 1 time repeating (Fig. S6 and S7), this study examined significantly elevated activities of all four types of enzymes by 31%–81% from *A. niger* incubations with the rice mutant straw, compared to the controls (without ultrasound) (Fig. 1F–I). Notably, under the optimal ultrasound treatment, all rice mutant samples exhibited consistently higher activities of the four enzymes than those of the WT at $p < 0.01$ level ($n = 3$), indicating that the optimal ultrasound treatment should be more effective for improving *A. niger* incubations compared to the *T. reesei*. Therefore, the optimal ultrasound treatment with rice mutant straw provides a novel and integrative biotechnology for consistently improved fungal secretions of lignocellulose-degradation enzymes with high activities and yields.

3.2. Synergistically enhanced biomass saccharification of three representative bioenergy plants by two fungi-secreted enzymes

To test the two fungi-secreted enzymes for biomass saccharification, our previously-established mild alkali (0.5% NaOH) pretreatments were performed with three representative bioenergy crops (eucalyptus, fern, rice), and the yields of hexoses (% cellulose) and total sugars (% dry matter) released from enzymatic hydrolyses of the pretreated lignocelluloses were determined (Fig. 3A). By supplying the enzymes secreted from *T. reesei* incubation with rice mutant under optimal ultrasound treatment, the three crops showed consistently raised hexoses and total sugars levels released from enzymatic hydrolyses of their pretreated lignocelluloses, compared to the controls (secreted enzymes without ultrasound treatment) or the commercial mixed-cellulase enzymes (Fig. 3B, C and Table S2). Notably, by combining the two fungi-secreted enzyme solutions at an optimal ratio of 1 (*T. reesei*) : 1/8 (*A. niger*), we

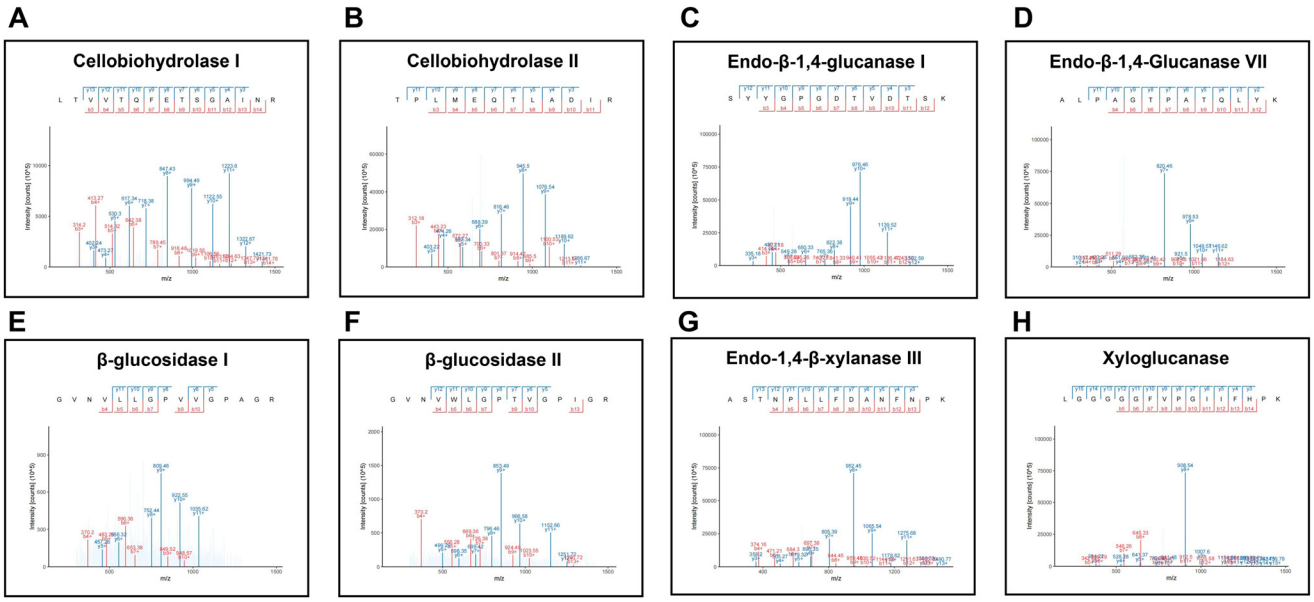

Fig. 2 (A–H) LC-MS/MS profiling of cellulases secreted by *T. reesei* incubation with the rice mutant under optimal ultrasound treatment.

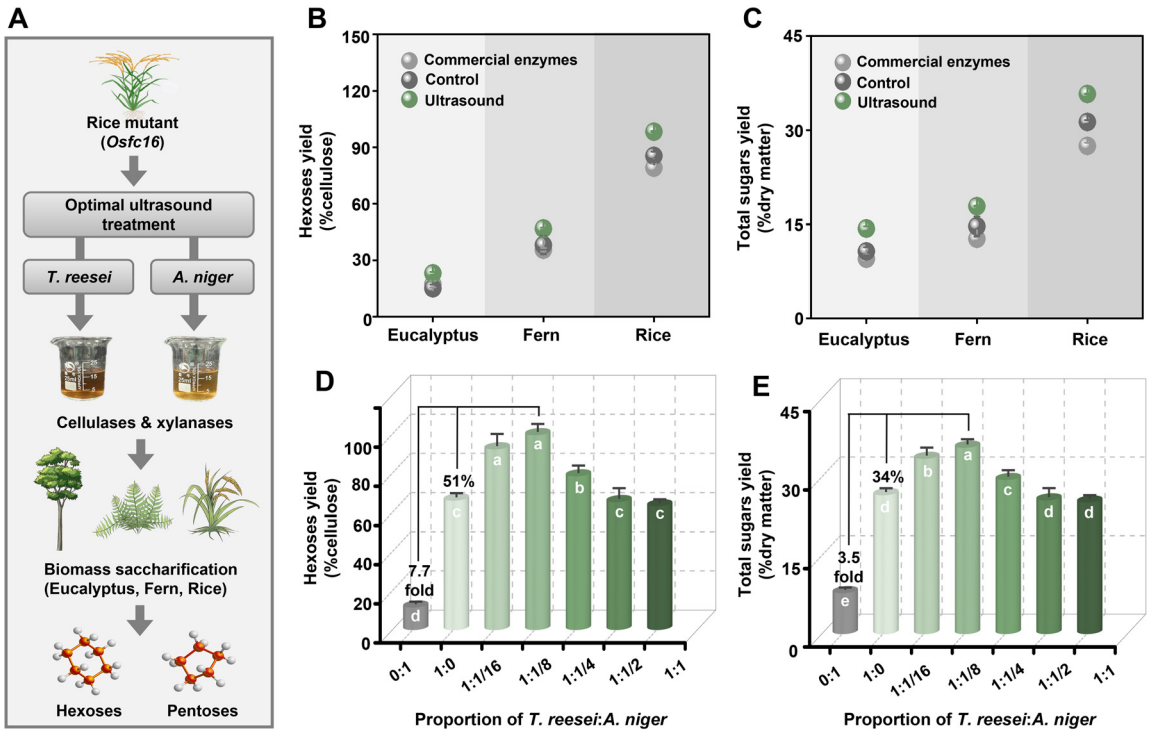

Fig. 3 Biomass saccharification of bioenergy crops using *T. reesei*- and *A. niger*-secreted enzymes and commercial mixed-cellulases: (A) general experimental procedure; (B and C) yields of hexoses and total sugars released from enzymatic hydrolysis of 0.5% NaOH-pretreated straw; (D and E) yields of hexoses and total sugars released from enzymatic hydrolysis of 0.5% NaOH-pretreated rice straw by incorporation of two fungi-secreted solutions in different proportions. Significant differences between samples were determined using one-way ANOVA: $p < 0.05$ ($n = 7$).

achieved near-complete biomass enzymatic saccharification. The hexoses yield reached 99% and total sugar yield reached 36% from enzymatic hydrolysis of mild alkali-pretreated rice straw. These yields represent significant increases of 51% and 34% for hexoses and total sugars, respectively, compared with using *T. reesei*-secreted enzymes alone, and increases of 7.7-fold and 3.5-fold compared with using *A. niger*-secreted enzymes alone (Fig. 3D, E and Fig. S8). The results thus

demonstrated a remarkably synergistic enhancement of biomass enzymatic saccharification from the optimal incorporation of two fungi-secreted enzymes, which accounted for a perfect compensation of four types of enzymes secreted from two fungi incubations with the rice mutant under optimal ultrasound treatments (Fig. 1). In addition, this study evaluated the potential global hexoses and pentoses yields (t per ha per year) released from enzymatic hydrolyses of alkali-pretreated lignocelluloses in eucalyptus and rice by incorporating two fungi-secreted enzymes, and the two crops respectively showed 15% and 52% increases of hexoses yield and 11% and 12% increases of pentoses (Table S3), indicating a potential application for high-yield sugar production on a large scale.[42,43]

3.3. Dynamically densified fungal mycelium and digested lignocellulose

To understand how the optimal ultrasound treatment could improve the two fungi incubations with rice straw for secreting lignocellulose-degradation enzymes with high yields and activities, we observed the growth of two fungi mycelium from a time-course cultivation under fluorescence microscopy (Fig. 4). During 3–7 days cultivations, the optimal ultrasound treatment consistently reduced the *T. reesei* mycelium lengths by 68%–78% relative to those of the control (without ultrasound) in both rice mutant and WT samples (Fig. 4B and C), which accounted for the observed much increased densities of *T. reesei* mycelium (Fig. 4A). Further, compared to the WT samples, the rice mutant samples presented the mycelium at higher densities in both ultrasound treatment and control. Accordingly, the incubated lignocelluloses exhibited much smaller sizes, and the optimal ultrasound treatment even caused more homogeneous residues than those of the controls in both rice mutant and WT samples. These phenomena should be attributed to synergistically mechanical and biological impacts of the sonication (shear forces, agitation, and cavitation) and enzymatic digestion, which could increase the number of accessible sites on the lignocellulose surfaces for feedback improvement of dissected-mycelium interactions with digested-lignocellulose residues. As a consequence, we determined significantly raised levels of soluble sugars (hexoses, pentoses) retained in the supernatants under optimal ultrasound treatment, which should be due to feedback-improved lignocellulose enzymatic hydrolysis (Fig. 5A and B). As the soluble sugars could serve as essential carbon sources for fungal growth, they should create a positive feedback circuit that enhances cellulase secretion. Moreover, the optimal ultrasound treatment caused significantly higher total

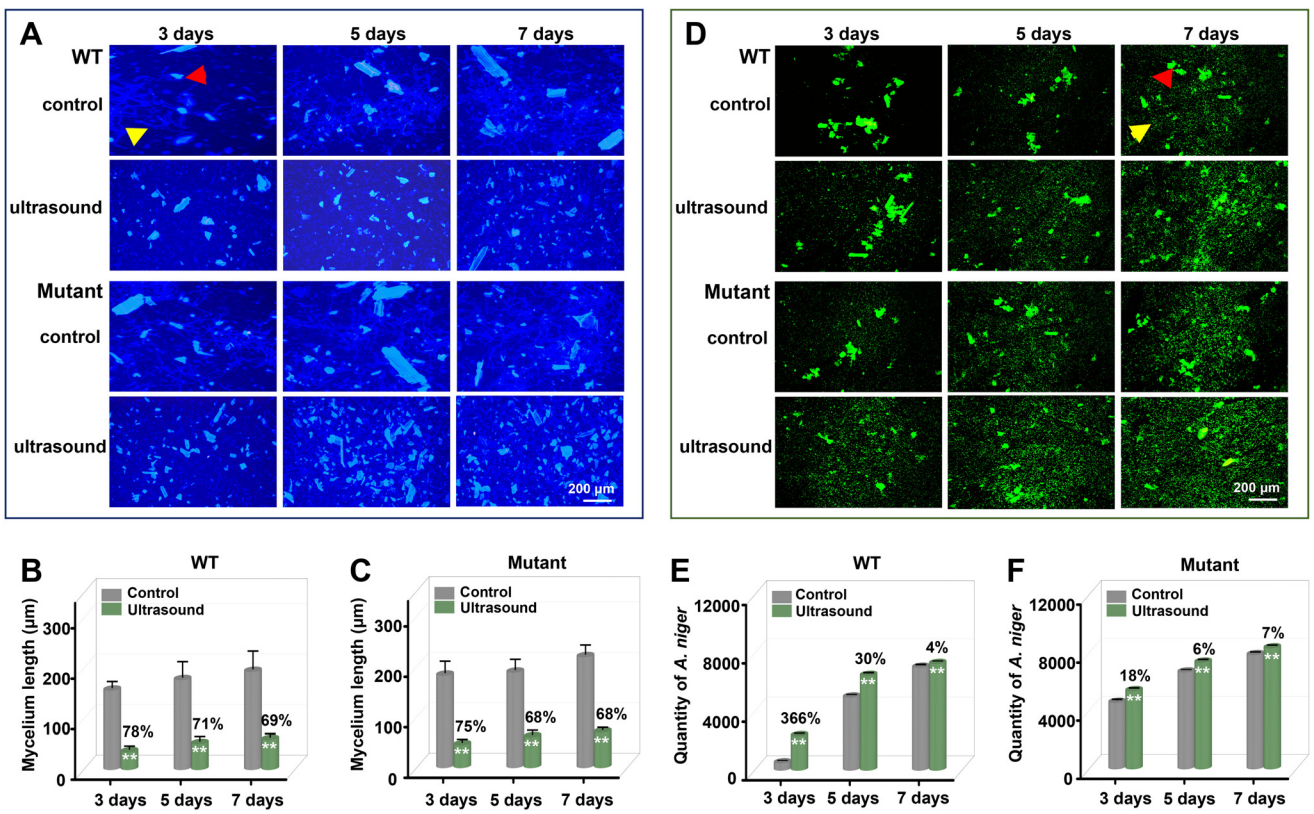

Fig. 4 Time course observations of fungal incubations under the optimal ultrasound treatment with rice mutant and WT straws: (A) fluorescence images of *T. reesei* mycelium (yellow arrow) and lignocellulose substrates (red arrow); (B and C) average length of randomly-selected 30 mycelium (n = 30); (D) fluorescence images of *A. niger* mycelium (yellow arrow) and lignocellulose substrates (red arrow); (E and F) quantity of *A. niger* mycelium under triplicate versions (n = 3); **significant difference at $p < 0.01$ level, and bar shows means ± SD.

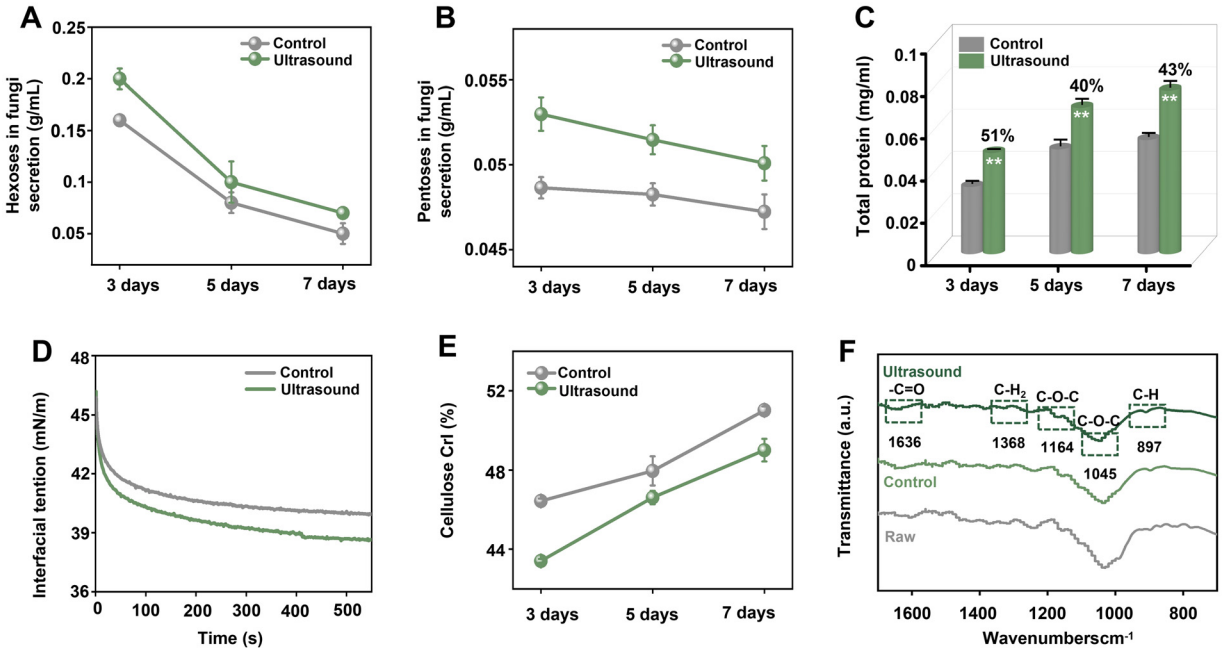

Fig. 5 Characterization of *T. reesei* incubation with the rice mutant under optimal ultrasound treatment for 3–7 days relative to the control (without ultrasound): (A and B) levels of hexoses and pentoses in the secreted solution; (C) total protein content of the secreted solutions; (D) dynamic interfacial tension of the secreted solutions after 7-day incubation; (E) CrI values of lignocelluloses after incubation; (F) FT-IR spectroscopic profiling of lignocellulose residues after 7-day incubation. Dot-box highlights altered peaks as annotated in Table S4, grey is raw straw, light green is lignocellulose residue after 7-day induction without ultrasound, and dark green is the residue after optimal ultrasound treatment after 7-day incubation. **Significant difference relative to the control at $p < 0.01$ levels ($n = 3$), bar shows mean ± SD.

protein levels than those of the controls by 40%–51% at $p < 0.01$ level ($n = 3$) from fungal incubation (Fig. 5C), which is consistent with the upgraded activities of lignocellulose-degradation enzymes secreted by *T. reesei* (Fig. 1). In addition, this study determined constantly reduced interfacial tension of the supernatants and CrI value of the lignocellulose residues from the optimal ultrasound treatment relative to the controls (Fig. 5D and E). FT-IR spectroscopic analysis also revealed distinctively altered chemical bonds (–C═O, C–H_2, C–O–C, and C–H) assigned to lignocellulose-associated functional groups (Fig. 5F and Table S4), further confirming the densified fungal mycelium and digested lignocelluloses.[44–49]

Meanwhile, we observed the growth of *A. niger* from 3–7 days cultivation with lignocelluloses of rice mutant and WT (Fig. 4D). Like *T. reesei* incubation, the optimal ultrasound treatment could also increase the densities of *A. niger* mycelium, compared to the controls at $p < 0.01$ levels ($n = 30$), but the rice mutant samples retained consistently higher mycelium densities than those of the WT (Fig. 4E and F). Notably, the optimal ultrasound treatment led to significantly reduced lignocellulose residues than those of the controls by 8%-21% at $p < 0.01$ levels ($n = 30$), and the rice mutant samples retained smaller residues relative to the WT (Fig. S9A and B), which were validated by significantly reduced cellulose CrI and DP values in the rice mutant samples under the optimal ultrasound treatment (Fig. S9C and D). Taken together, the optimal ultrasound treatment not only improved the growth of the two fungi for high-density mycelium, but it also enhanced lignocellulose digestion, which enabled effective fungal interactions with the recalcitrance-reduced lignocellulose of the rice mutant as a synergistic enhancement for efficient secretion of lignocellulose-degradation enzymes.

3.4. Contrasting porosities of nano-lignocellulose and nanocarbon

Given that fungal incubation retained substantial amounts of lignocellulose residues, this study characterized their porosities as potentially valuable bioproducts (Fig. 6). Using the previously-established AFM approach,[9,20] we observed a distinct pore morphology of the lignocellulose residues for the rice mutant and WT samples examined (Fig. 6A). By measuring the average pore sizes of 50 randomly selected residues, this study identified the smallest pore size in the rice mutant sample under optimal ultrasound treatment (Fig. 6B). As a comparison, the two rice mutant samples exhibited significantly smaller pore sizes than those of WT by 43% and 57% at $p < 0.01$ levels ($n = 50$), and the ultrasound treatment remarkably reduced the pore sizes by 2.9 and 3.8 folds, respectively, in the rice mutant and WT samples, which were validated by the significantly reduced cellulose CrI and DP values of the nano-lignocelluloses examined in the rice mutant sample under optimal ultrasound treatment (Fig. 6C and D).

Furthermore, the nano-lignocellulose residues from *T. reesei* incubations were employed to generate biocarbon

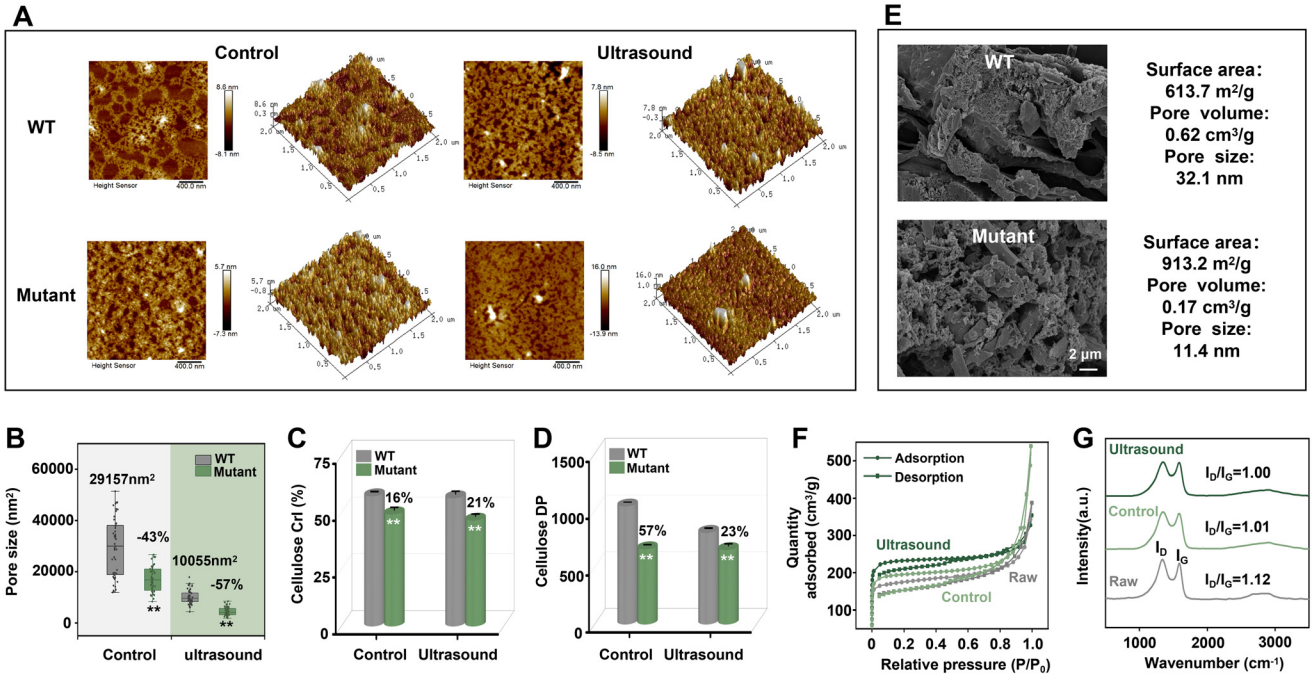

Fig. 6 Characterization of the nano-lignocelluloses and nano-carbons during *T. reesei* incubation with rice mutant under optimal ultrasound treatment: (A) AFM images of nano-lignocelluloses; (B) average pore sizes of 50 randomly selected nano-lignocelluloses (n = 50); (C and D) nano-lignocellulose CrI and DP values (n = 3); (E) SEM images and BET porosity of nano-carbons; (F and G) BET and Raman spectra profiling of nano-carbons; WT is wild type of rice mutant; raw is rice raw straw without fungal incubation; control is fungal incubation without ultrasound treatment; **significant difference at $p < 0.01$ level; bar shows mean ± SD.

materials by performing $FeCl_2{\cdot}4H_2O$-activated thermal-chemical conversion at 1000 °C. Under a typical BET assay conducted by measuring the N_2 adsorption/desorption isotherms,[29,50] the biocarbon generated from the rice mutant residues exhibited different porosity characteristics, such as a 49% increase in the surface area and a reduction in the pore size and volume by 3.6 and 2.8 folds compared to the WT sample (Fig. 6E), which should be due to a synergistic impact from *T. reesei* incubation with desirable rice mutant under optimal ultrasound treatment. To test this hypothesis, we compared this biocarbon with two other biocarbon materials generated from raw straw and the *T. reesei* incubation residue of rice mutant without ultrasound treatment (control). As a result, this biocarbon sample exhibited a significantly increased surface area and reduced pore volume and size at $p < 0.01$ levels (n = 3) compared to the raw straw and control samples, but the control sample retained a higher surface area and lower pore volume and size than observed for the raw straw samples (Fig. 6F and Fig. S10A–C), which should be attributed to the synergistic role of the effective integration of *T. reesei* incubation with the rice mutant under optimal ultrasound treatment. Although Raman spectroscopic profiling showed a characteristic G peak for a graphene-like carbon assembly in all three samples (Fig. 6G), a sharper XRD peak was observed at the (002) crystal plane, indicating a highly crystalline and well-ordered structure with graphitic characteristics in the ultrasound biocarbon sample (Fig. S10D).[51–54] The XPS analysis further revealed that the ultrasound biocarbon consists of 90.6% carbon, 9.17% oxygen and 0.23% Fe, suggesting that $FeCl_2{\cdot}4H_2O$ primarily served a catalytic role in biocarbon assembly (Fig. S10E). In addition, four characteristic peaks of the C 1s spectrum were identified as corresponding to sp^2–bonded carbon (284.6 eV), sp^3–C (285.7 eV), C–O (286.3 eV), and C═O (287.1 eV), and two distinct peaks of the O 1s spectrum were assignable to C–O (531.4 eV) and C═O (532.9 eV) (Fig. S10F and G). These results thus confirmed that a graphene-like nanocarbon was typically assembled with distinctly improved porosity by the cascading integration of *T. reesei* incubation with rice mutant under optimal ultrasound treatment.

3.5. Remarkably upgraded dye adsorption and electrochemical conductivity

As the biocarbon derived from rice mutant straw under optimal ultrasound treatment exhibited distinct porosity compared to all other biocarbon samples examined, this study compared their adsorption capacities for two industrial dyes, methylene blue (MB) and Congo red (CR) (Fig. 7). In general, the ultrasound biocarbon showed the highest adsorption capacities with the two dyes of all six samples examined (Fig. 7A and B), which should be attributed to its highest surface area and lowest pore volume and size. In particular, the three mutant samples exhibited significantly higher adsorption capacities than those of the WT, and the control

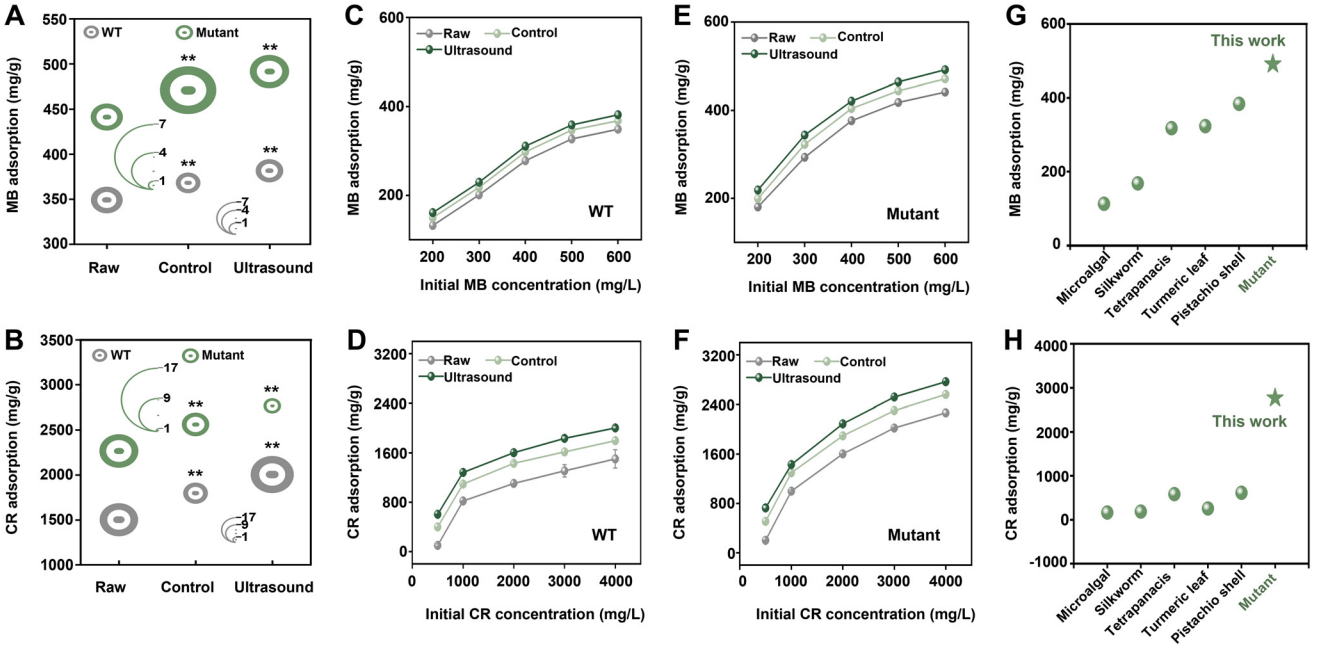

Fig. 7 Upgraded dye adsorption of the nano-carbon generated from the nano-lignocellulose residues after *T. reesei* incubation with rice mutant under optimal ultrasound treatment: (A and B) methylene blue (MB) and Congo red (CR) adsorptive capacities; (C–F) MB and CR adsorptive trends; (G and H) comparison of dyes adsorptions with the biocarbon samples as previously generated from five other biological materials. WT is wild type of rice mutant; raw is rice raw straw without fungal incubation; and Control is fungal incubation without ultrasound treatment; **significant difference at $p < 0.01$ level ($n = 3$); bar shows mean ± SD.

samples were determined with consistently increased adsorptions compared to the raw straw samples at $p < 0.01$ levels ($n = 3$) (Fig. 7C–F). Notably, the desirable biocarbon obtained in this study showed much higher adsorptive capacities with MB (492 mg g^{-1}) and CR (2766 mg g^{-1}), compared to the biocarbon samples previously produced from five other biological materials for adsorption of MS (113 mg/g-384 mg g^{-1}) and CR (164 mg g^{-1}–615 mg g^{-1}) (Fig. 7G and H), revealing that the optimal biocarbon could be generated from the desirable nano-lignocellulose residues retained from fungal incubation with rice mutant under optimal ultrasound treatment.[55–59] To test this assumption, the desirable nano-lignocellulose residues were directly utilized as biosorbents for dye adsorption (Fig. 8). As a result, the desirable biosorbents showed consistently higher adsorptive capacities with MB and CR than those of the raw straw and control samples, and all rice mutant samples remained significantly higher adsorptions compared to the WT at $p < 0.01$ level ($n = 3$), which were consistent with the biocarbon adsorption trends.

To extend biocarbon function, the electrochemical performance of the biocarbon material was evaluated in a three-electrode supercapacitor system (Fig. 9). Based on the cyclic voltammogram test at a scan rate of 100 mV s^{-1}, the optimal ultrasound biocarbon showed the highest current density compared to other two biocarbon samples from raw rice straw and control treatment (without ultrasound) (Fig. 9A and B). Meanwhile, galvanostatic charge–discharge (GCD) measurements exhibited symmetrical isosceles triangular curves from all biocarbon samples, indicating a typically favorable electrochemical behavior,[60–62] and the ultrasound biocarbon exhibited prolonged discharge durations compared to the other two biocarbon samples (Fig. 9C and D). Under electrochemical impedance spectroscopy, the ultrasound biocarbon exhibited the lowest resistance, suggesting accelerated ion diffusion kinetics and abundant adsorption/desorption sites for electrochemical reactions (Fig. 9E and F).[63–65] Particularly, the ultrasound biocarbon showed consistently higher specific capacitances than those of other biocarbon samples, and also maintained a notable capacitance retention rate of 25.5%, even at a high current density loading (20 A g^{-1}) (Fig. 9G and H). Meanwhile, when the materials prepared in this study were compared with other biocarbon samples previously generated from other bioresources, this biocarbon sample showed a higher specific capacitance (Tables 1 and 2).[66–75] However, an advanced technology to maximize biocarbon performance by using the desirable nano-lignocellulose residues obtained in this study remains to be explored.

3.6. A proposed mechanism model for the synergistic improvements achieved by integrative biotechnology

Based on all the findings, a mechanistic model was proposed to elucidate how integrative biotechnology could cause a synergistic enhancement of cellulase and sugar production and a cascading improvement of biosorbent and biocarbon materials with increased dye adsorption capacity and electrochemical conductivity (Fig. 10). (I) Because the rice OsCesA9 site-mutant

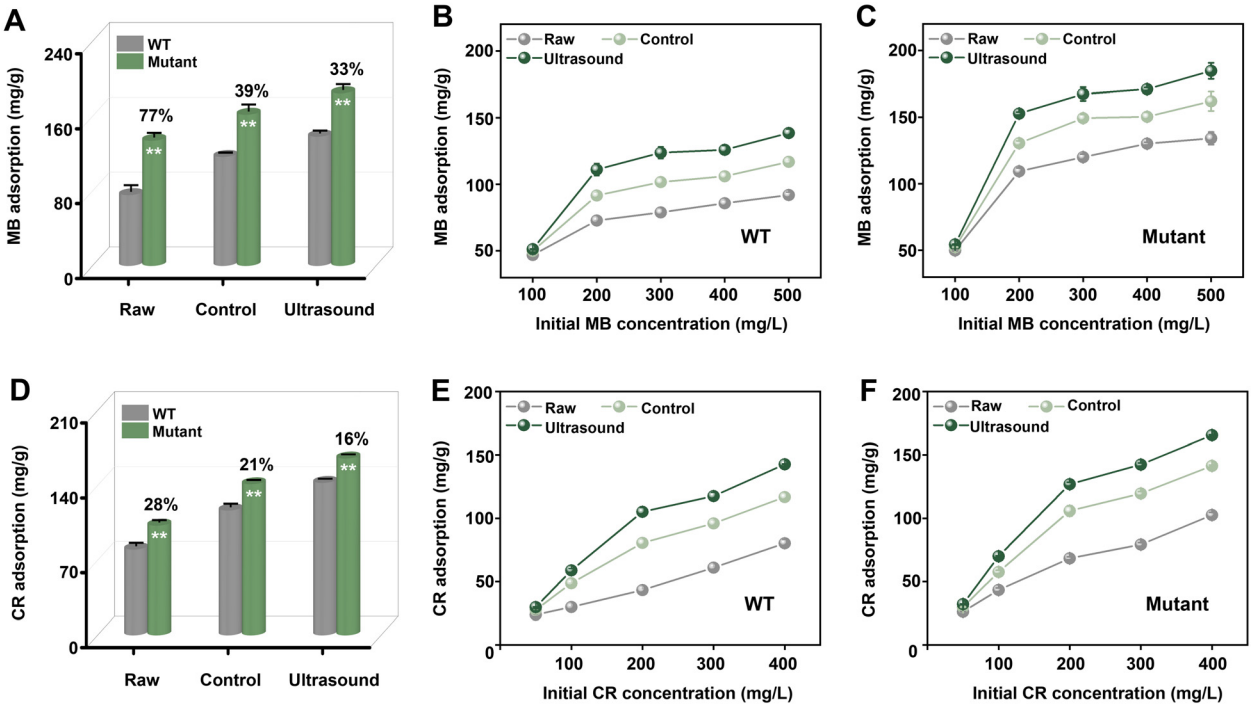

Fig. 8 Characterization of biosorbents for dye adsorption directly using the lignocellulose residues from *T. reesei* incubation with rice straw under optimal ultrasound treatment relative to the control (without ultrasound): (A–C) MB adsorption; (D–F) CR adsorption. Raw sample from rice raw straw without any fungal incubation; **significant difference between mutant and WT at $p < 0.01$ level ($n = 3$); and bar shows mean ± SD.

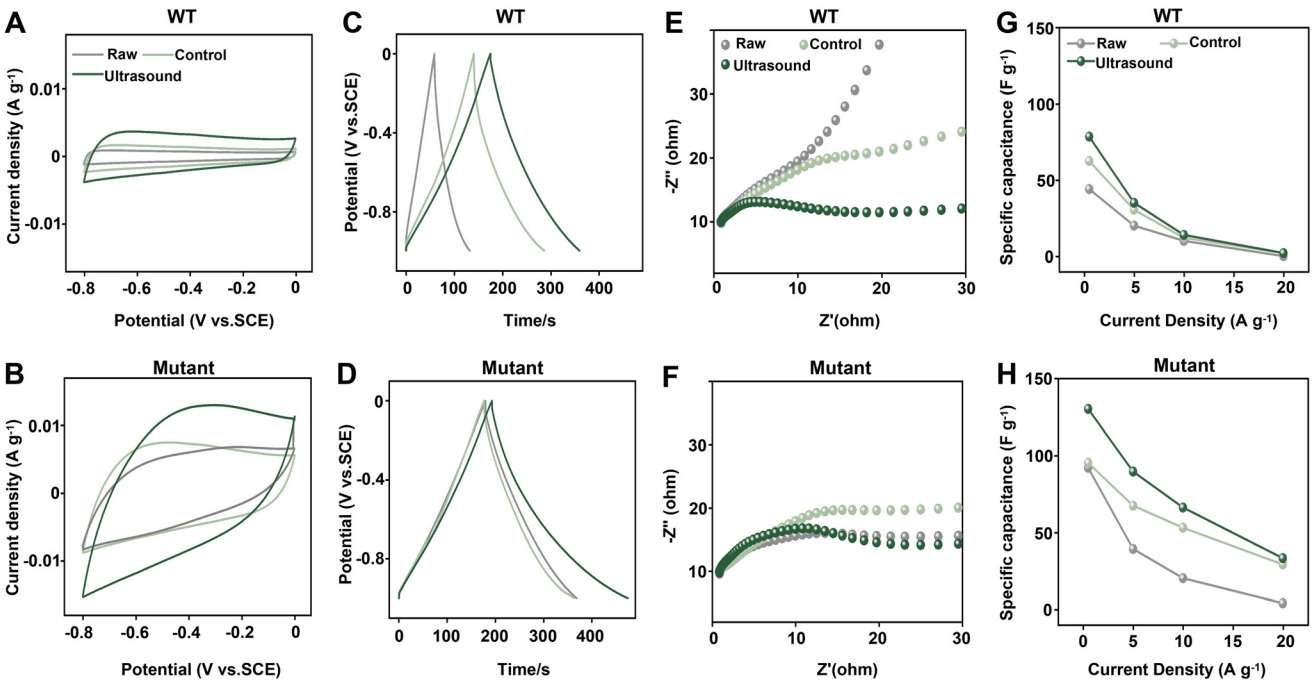

Fig. 9 Improved electrochemical conductivity of the nano-carbons generated from the nano-lignocellulose residues after *T. reesei* incubation with rice mutant under optimal ultrasound treatment: (A and B) cyclic voltammetry curves for current density; (C and D) galvanostatic charge/discharge curves for potential value; (E and F) Nyquist plot by electrochemical impedance spectroscopy; (G and H) specific capacitance at different current densities. WT is the wild type of rice mutant; raw is rice raw straw without fungal incubation; and Control is fungal incubation without ultrasound treatment.

Table 1 Comparison of specific capacitance of the biochar samples in this study with those in previous reports

Material	Activation method	Current density (A g^{-1})	Specific capacitance (F g^{-1})	Ref.
Rice mutant residue	**Ultrasound**	**0.5**	**130.2**	**This study**
Jamun seed	HCl + CO_2	0.5	38	Rawat *et al.* (2023)[66]
Anthracite coal	KOH	0.5	80.5	Ding *et al.* (2019)[67]
Cotton stalk	KOH	0.5	115	Tian *et al.* (2021)[68]
Wood	Cu/As/Cr + KOH	0.5	76.7	Huang *et al.* (2024)[69]
Pine nut shell	Steam	0.5	128	Qin *et al.* (2019)[70]

Table 2 Comparison of the increased rates of specific capacitance of the biochar samples in this study with those in previous reports

Material	Activation method	Current density (A g^{-1})	Increased rates of specific capacitance (%)	Ref.
Rice mutant residue	**Ultrasound**	**0.5**	**196**	**This study**
Loofah sponge	Pre-burning	0.5	99	Ye *et al.* (2024)[71]
Ethyl cellulose	Gamma radiation	0.5	104	Adhamash *et al.* (2020)[72]
Fruit bunch	TiO_2	0.5	126	Gunasekaran *et al.* (2025)[73]
Silk worms	Copper phosphate	0.5	59	Justinabraham *et al.* (2023)[74]
Bamboo residue	Fermentation	0.5	13	Wang *et al.* (2024)[75]

(*Osfc16*) is of the length-reduced CNFs assembly, accounting for high-density amorphous cellulose chains,[9,32] it provides many more breakpoints for initial fungal interaction and digestion of lignocelluloses, which should generate more soluble hexoses as a carbon source and facilitate fungal growth and feedback-like enzyme secretion. As the site-mutants of three essential cellulose synthase isoforms (OsCesA4, 7, 9) have been generated for diverse CNFs substrates,[20,76] it offers the option to explore more ideal substrates for more active fungal incubation. (II) As the optimal ultrasound treatment could facilitate fungal interactions with rice CNFs, it should have an integrative impact on fungal secretion of lignocellulose-degradation enzymes with high activity. Meanwhile, while the optimal ultrasound treatment dissects fungal mycelium, it is more favorable for fungal interaction with CNFs at high density due to its highly homogeneous distribution, which should facilitate a synergistic enhancement of cellulase secretion in high yield. It also reveals a potential for genetic engineering of fungal strains for effective mycelium dissection under optimal ultrasound treatment in the future. (III) Although ultrasound treatment requires energy input, the optimal conditions (108 W, 4 min, 1 t) represented a short-duration and high-efficacy intervention within the multi-day cultivation. The enhancements of biomass saccharification and cellulase production with high-performance bioproducts justify the energy input *via* the cascading system, but future scale-up work could further optimize the energy balance through pulsed operation or reactor design. (IV) From a mass-balance perspective, this strategy aims at near-complete utilization of the input biomass: lignocelluloses can be converted into fermentable sugars *via* fungal-induced cellulase secretion and enzymatic hydrolysis of energy plants,[77] whereas the solid residues are entirely transformed into functional materials (biosorbents and biocarbon). This demonstrates the inherent potential of the integrated design for resource efficiency and waste minimization, laying the foundation for a sustainable circular bioeconomy. (V) Even though the two fungi (*T. reesi*, *A. niger*) incubations under optimal ultrasound treatment could distinctly enhance enzyme secretions, the activities of four major lignocellulose-degradation enzymes are perfectly compensated between the two fungal secretions, enabling another synergistic enhancement of biomass enzymatic saccharification in bioenergy crops. The optimal incorporation proportion of the two fungal-secreted enzymes will thus provide insights into enzymatic catalysis for complete lignocellulose hydrolysis into fermentable sugars. (VI) Since the desirable residues retained from the fungal incubation are composed of dissected mycelium and size-reduced nano-lignocelluloses, they could be directly utilized as effective biosorbents for efficient adsorption of two distinct industrial dyes (MB, CR), primarily cascading a green technology for value-added bioproduction with zero-biomass release. (VII) By further subjecting the desirable nano-lignocelluloses to $FeCl_2{\cdot}4H_2O$-activated thermal-chemical conversion, highly porous biocarbon can be readily generated. This biocarbon exhibits 4- to 17-fold higher adsorption capacities for methylene blue (MB) and Congo red (CR) compared to the original biosorbent, and shows a 2-fold improvement in specific capacitance for electrochemical conductivity relative to biocarbon directly produced from raw rice straw. Thus, the integrative biotechnology of plant CNFs and dissected fungal mycelium enables a cascading and synergistic improvement for optimal bioeconomy options.

To align this cascading strategy with the principles of green chemistry and circular bioeconomy, future management of its aqueous waste streams is required. The environmental footprint can be reduced by implementing the following recovery and recycling approaches: (I) spent fermentation broth: After fungal incubation, the liquid fraction containing soluble sugars and proteins could be recovered as nutrient sources for subsequent fermentation or microbial growth media. (II) Alkali pretreatment liquor: The dilute NaOH (0.5% w/v) could be partially recovered and reused in subsequent pretreatment cycles following pH adjustment, minimizing both fresh alkali

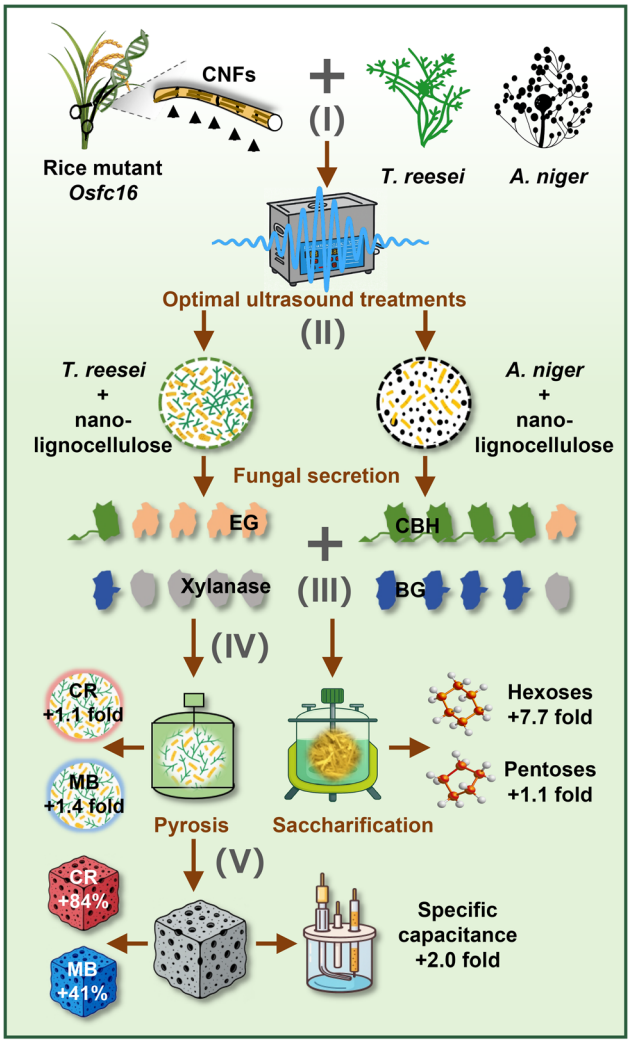

Fig. 10 Mechanistic model of the integrative biotechnology for synergistic enhancement of cellulase and sugar production and high-performance biocarbon generation. The black arrow highlights the amorphous cellulose chain, and "+" indicates increased rate relative to the raw straw of rice WT without fungal incubation.

consumption and effluent load. (III) Acid wash from biocarbon generation: the HCl used for removing metal ions can be reused or neutralized with a base for safe disposal, and the Fe-rich solution is also considered for iron salt recovery as $Fe(OH)_3$ or Fe_2O_3. In conclusion, incorporating these valorizations of the major process streams would potentially transform waste components into resources, thereby enhancing the overall sustainability and economic viability of the proposed integrated biorefinery.

4. Conclusions

This study developed an integrative biotechnology system for the secretion of lignocellulose-degradation enzymes with high activities and yields from two distinct fungi (*T. reesei* and *A. niger*) incubations with rice natural mutant (*Osfc16*) straw under optimal ultrasound treatment. By optimal incorporation of two fungi-secreted enzymes, this work demonstrated a synergistic enhancement for near-complete biomass saccharification, even though the mild alkali pretreatment was conducted with crop straw. Despite this, the remaining residues composed of digested lignocelluloses and dissected mycelium were directly utilizable as desirable biosorbents for dye adsorption; they were used to simply generate highly porous biocarbon materials either for exceptionally high dye adsorption or for high-performance electrode nanocarbons for supercapacitors. A mechanistic model is proposed to elucidate how the novel biotechnology enables synergistic enhancements of cellulase and sugar production, leading to cascading improvements in the biosorbent and biocarbon performance for industrial dye removal and enhanced electrochemical conductivity by integrating genetically engineerable crop straw rich in CNF assemblies with high-density, ultrasound-dissectible fungi mycelium. To fully quantify its environmental footprint and industrial viability, a complete life-cycle assessment will provide a comprehensive assessment based on scaled-up process data.

Author contributions

Hao Peng: investigation, methodology, visualization, writing – original draft. Peng Liu: software, formal analysis, methodology. Jingyuan Liu, Junsheng Yu, Boyang He, Yujing Yang, Hua Yu, and Heng Kang: supervision, methodology, formal analysis. Mengzhou Zhou, Wanbin Zhu, and Muhammad Nauman Aftab: investigation, validation. Yanting Wang, Chunxiang Fu, and Liangcai Peng: conceptualization, methodology, funding acquisition, writing – review and editing.

Conflicts of interest

There are no conflicts to declare.

Data availability

The author confirms that the data supporting the findings of this study are available within the article.

Supplementary information (SI) is available. Supplementary Information is available and includes additional experimental details, supplementary figures (Fig. S1–S10) and tables (Table S1–S4), covering rice mutant characterization, ultrasound optimization, enzyme identification, biomass saccharification data, and biocarbon analysis. See DOI: https://doi.org/10.1039/d5gc06304c.

Acknowledgements

This work was supported in part by the Hubei Provincial Natural Science Foundation of China for Excellent Young

Scientists (No. 2024AFA100), the National Natural Science Foundation of China (No. 32470273; No. 32570317; No. 32170268; and No. 32101701), the National 111 Project of the Ministry of Education of China (No. D17009), and the Initiative Grant of Hubei University of Technology for High-level Talents (No. GCC20230001).

References

1 P. Liu, A. Li, Y. M. Wang, Q. M. Cai, H. Z. Yu, Y. Q. Li, H. Peng, Q. Li, Y. T. Wang, X. Y. Wei, R. Zhang, Y. Y. Tu, T. Xia and L. C. Peng, *Renewable Energy*, 2021, **174**, 799–809.
2 S. Sajid, O. K. Zveushe, V. R. Dios, F. Nabi, Y. K. Lee, A. R. Kaleri, L. Ma, L. Zhou, W. Zhang, F. Q. Dong and T. Han, *Bioresour. Technol.*, 2022, **354**, 127150.
3 D. J. Cosgrove, *Nat. Rev. Mol. Cell Biol.*, 2023, **25**, 340–358.
4 M. Wang, Y. X. Wang, J. Y. Liu, H. Yu, P. Liu, Y. J. Yang, D. Sun, H. Kang, Y. T. Wang, J. F. Tang, C. X. Fu and L. C. Peng, *Green Carbon*, 2024, **2**, 164–175.
5 H. L. Wang, S. F. Li, L. M. Wu, W. H. Zou, M. L. Zhang, Y. M. Wang, Z. Y. Lv, P. Chen, P. Liu, Y. J. Yang, L. C. Peng and Y. T. Wang, *Green Chem.*, 2025, **27**, 9127.
6 H. Yu, G. F. Zhang, J. Y. Liu, P. Liu, H. Peng, Z. P. Teng, Y. Li, X. F. Ren, C. X. Fu, J. F. Tang, M. Li, Y. T. Wang, L. Q. Wang and L. C. Peng, *J. Adv. Res.*, 2025, **78**, 1–9.
7 J. Kari, G. A. Molina, S. K. Schaller, C. Schiano-di-Cola, S. J. Christensen, S. F. Badino, T. H. Sørensen, N. S. Røjel, M. B. Keller, N. R. Sørensen, B. Kolaczkowski, J. P. Olsen, K. B. R. M. Krogh, K. Jensen, A. M. Cavaleiro, G. H. J. Peters, N. Spodsberg, K. Borch and P. Westh, *Nat. Commun.*, 2021, **12**, 3847.
8 R. R. Singhania, H. A. Ruiz, M. K. Awasthi, C. D. Dong, C. W. Chen and A. K. Patel, *Renewable Sustainable Energy Rev.*, 2021, **151**, 111622.
9 R. Zhang, Z. Hu, Y. T. Wang, H. Z. Hu, F. C. Li, W. Li, A. Ragauskas, T. Xia, H. Y. Han, J. F. Tang, H. Z. Yu, B. Q. Xu and L. C. Peng, *Nat. Commun.*, 2023, **14**, 1100.
10 S. Pant, N. P. Ritika, A. Ghati, D. Chakraborty, M. R. Maximiano, O. L. Franco, A. M. Mandal and A. Kuila, *Biotechnol. Adv.*, 2022, **60**, 108022.
11 C. B. Xu, T. Xia, H. Peng, P. Liu, Y. H. Wang, Y. T. Wang, H. Kang, J. F. Tang, M. N. Aftab and L. C. Peng, *Bioresour. Technol.*, 2023, **376**, 128844.
12 M. Schuster, S. Kilaru, H. A. B. Wösten and G. Steinberg, *Nat. Commun.*, 2025, **16**, 4402.
13 E. Papadaki, K. N. Kontogiannopoulos, A. N. Assimopoulou and F. T. Mantzouridou, *Bioresour. Technol.*, 2020, **309**, 123317.
14 S. G. Karp, A. M. Rozhkova, M. V. Semenova, D. O. Osipov, S. T. Z. Pauli, O. A. Sinitsyna, I. N. Zorov, L. P. S. Vandenberghe, C. R. Soccol and A. P. Sinitsyn, *Bioresour. Technol.*, 2021, **330**, 124888.
15 G. B. Santos, Á.SF. Filho, J. R. S. Rodrigues and R. R. Souz, *J. Environ. Manage.*, 2022, **305**, 114431.
16 P. Liu, Y. H. Wang, H. Kang, Y. T. Wang, H. Yu, H. Peng, B. Y. He, C. B. Xu, K. Z. Jia, S. L. Liu, T. Xia and L. C. Peng, *Int. J. Biol. Macromol.*, 2024, **278**, 134524.
17 J. Y. Liu, X. Zhang, H. Peng, T. Q. Li, P. Liu, H. R. Gao, Y. T. Wang, J. F. Tang, Q. Li, Z. Qi, L. C. Peng and T. Xia, *Molecules*, 2023, **28**, 2060.
18 X. Y. Huang, L. Deng, X. Zhang, X. Q. Zhao, C. G. Liu and F. W. Bai, *Green Chem.*, 2025, **27**, 2733–2742.
19 H. Peng, W. Y. Zhao, J. Y. Liu, P. Liu, H. Z. Yu, J. Deng, Q. M. Yang, R. Zhang, Z. Hu, S. L. Liu, D. Sun, L. C. Peng and Y. T. Wang, *Green Chem.*, 2022, **24**, 2975–2987.
20 R. Zhang, Z. Hu, H. Peng, P. Liu, Y. M. Wang, J. Y. Li, J. Lu, Y. T. Wang, T. Xia and L. C. Peng, *Green Chem.*, 2023, **25**, 1096–1106.
21 Y. H. Ai, H. L. Wang, P. Liu, H. Yu, M. D. Sun, R. Zhang, J. F. Tang, Y. T. Wang, S. Q. Feng and L. C. Peng, *Sci. Bull.*, 2024, 3815–3819.
22 L. Khedmat, A. Izadi, V. Mofid and S. Y. Mojtahedi, *Carbohydr. Polym.*, 2020, **229**, 115474.
23 E. C. Gaudino, G. Grillo, S. Tabasso, L. Stevanato, G. Cravotto, K. Marjamaa, V. Pihlajaniemi, A. Koivula, N. Aro, J. Uusitalo, J. Ropponen, L. Kuutti, P. Kivinen, H. Kanerva, A. Arshanitsa, L. Jashina, V. Jurkjane, A. Andersone, T. Dreyer and G. Schories, *J. Cleaner Prod.*, 2022, **380**, 134897.
24 V. Z. Ong and T. Y. Wu, *Renewable Sustainable Energy Rev.*, 2020, **132**, 109924.
25 E. M. M. Flores, G. Cravotto, C. A. Bizzi, D. Santos and G. D. Iop, *Ultrason. Sonochem.*, 2021, **72**, 105455.
26 V. Sharma, P. Nargotra, S. Sharma and B. K. Bajaj, *Renewable Energy*, 2021, **163**, 1910–1922.
27 Z. Hu, Q. Li, Y. Y. Chen, T. Q. Li, Y. M. Wang, R. Zhang, H. Peng, H. L. Wang, Y. T. Wang, J. F. Tang, M. N. Aftab and L. C. Peng, *Bioresour. Technol.*, 2023, **369**, 128437.
28 Y. S. Fu, H. R. Gao, H. Yu, Q. M. Yang, H. Peng, P. Liu, Y. Q. Li, Z. Hu, R. Zhang, J. Y. Li, Z. Qi, L. Q. Wang, L. C. Peng and Y. T. Wang, *Renewable Energy*, 2022, **200**, 1371–1381.
29 Y. T. Wang, H. Y. Zhang, Y. N. Li, H. Yu, D. Sun, Y. J. Yang, R. Zhang, L. Yu, F. Ma, N. M. Aftab, L. C. Peng and Y. T. Wang, *Int. J. Biol. Macromol.*, 2025, **291**, 138865.
30 T. K. Ghose, *Pure Appl. Chem.*, 1987, **59**, 257–268.
31 M. M. Bradford, *Anal. Biochem.*, 1976, **72**, 248–254.
32 H. Yu, M. Hu, Z. Hu, F. Liu, H. Z. Yu, Q. M. Yang, H. R. Gao, C. B. Xu, M. L. Wang, G. F. Zhang, Y. Wang, T. Xia, L. C. Peng and Y. T. Wang, *Carbohydr. Polym.*, 2022, **286**, 119298.
33 T. Q. Li, H. Peng, B. Y. He, C. Y. Hu, H. Y. Zhang, Y. N. Li, Y. J. Yang, Y. T. Wang, M. M. A. Bakr, M. Z. Zhou, L. C. Peng and H. Kang, *Int. J. Biol. Macromol.*, 2024, **264**, 1304484.
34 Y. N. Li, B. Y. He, H. Y. Zhang, J. Y. Liu, S. F. Li, H. L. Wang, H. Peng, Y. T. Wang, J. Dai, Y. T. Wang, L. C. Peng and H. Kang, *Ind. Crops Prod.*, 2024, **222**, 119924.
35 X. Y. Su, S. Bai, Q. Y. Xu, S. Xu, X. F. Liu, Z. Xu and N. Zhang, *Int. J. Biol. Macromol.*, 2025, **310**, 143179.

36 Q. Zhou, Z. J. Zhao, L. T. Wang, J. D. Wang, L. N. Fu, J. H. Cui, G. S. Liu, J. Yang and Y. J. Fu, *J. Bioresour. Bioprod.*, 2025, **10**, 224–238.
37 H. Fang, C. F. Li, J. J. Zhao and C. Zhao, *Biotechnol. Bioprocess Eng.*, 2021, **26**, 517–528.
38 M. L. Xiao, Y. M. Wang, Y. Wang, X. Yan, Z. H. Zhu, E. N. Tian, C. S. Yang, E. D. Ma, G. Zou, Z. H. Zhou and P. P. Wang, *Green Chem.*, 2023, **25**, 7362–7371.
39 J. Y. Si, C. R. Yang, Y. Chen, J. H. Xie, S. L. Tian, Y. A. Cheng, X. B. Hu and Q. Yu, *Food Chem.*, 2023, **407**, 135149.
40 C. Y. Liang, Y. Long, W. Wang, Y. Zhang, S. Y. Xing, Z. X. Chen and W. Qi, *Renewable Energy*, 2025, **240**, 122158.
41 V. Nimker, A. K. Patel, C. W. Chen, B. S. Giri, C. D. Dong and R. R. Singhania, *Int. J. Biol. Macromol.*, 2025, **318**, 145133.
42 E. F. Elli, P. C. Sentelhas, C. H. Freitas, R. L. Carneiro and C. A. Alvares, *For. Ecol. Manage.*, 2019, **450**, 117493.
43 S. Q. Xu, R. Wang, T. Gasser, P. Ciais, J. Peñuelas, Y. Balkanski, O. Boucher, I. A. Janssens, J. Sardans, J. H. Clark, J. J. Cao, X. F. Xing, J. M. Chen, L. Wang, X. Tang and R. H. Zhang, *Nature*, 2022, **609**, 299–306.
44 M. Balat, *Energy Convers. Manage.*, 2011, **52**, 858–875.
45 C. F. Xu, S. Hu, J. Xiang, L. Q. Zhang, L. S. Sun, C. Shuai, Q. D. Chen, L. M. He and E. M. A. Edreis, *Bioresour. Technol.*, 2014, **154**, 313–321.
46 H. P. Guo, C. T. Hong, X. M. Chen, Y. X. Xu, Y. Liu, D. A. Jiang and B. S. Zheng, *PLoS One*, 2016, **11**, 0153475.
47 A. Baum, M. Dominiak, S. Vidal-Melgosa, W. G. T. Willats, K. M. Søndergaard, P. W. Hansen, A. S. Meyer and J. D. Mikkelsen, *Food Bioprocess Technol.*, 2017, **10**, 143–154.
48 Z. J. Cai, B. L. Ji, K. L. Yan and Q. Zhu, *Polymers*, 2019, **11**, 2071.
49 H. C. Ong, W. H. Chen, Y. Singh, Y. Y. Gan, C. Y. Chen and P. L. Show, *Energy Convers. Manage.*, 2020, **209**, 112634.
50 C. K. Xia, S. Surendran, S. Ji, D. Kim, Y. Chae, J. Kim, M. Je, M. K. Han, W. S. Choe, C. H. Choi, H. Choi, J. K. Kim and U. Sim, *Carbon Energy*, 2022, **4**, 491–505.
51 S. Zhang, Q. F. Liu, H. Zhang, R. J. Ma, K. Li, Y. K. Wu and B. J. Teppen, *Carbon*, 2020, **157**, 714–723.
52 H. Li, W. C. Liu, J. X. Lu, Y. Lu, S. L. Shi, Z. Wang, Q. Ye and Z. Z. Jia, *Int. J. Min. Sci. Technol.*, 2023, **33**, 919–926.
53 B. Antil, Y. Elkasabi, G. D. Strahan and R. L. V. Wal, *Carbon*, 2024, **232**, 119770.
54 L. C. Meyer, A. K. Thiagarajan, A. Koposov and A. Balducci, *Energy Storage Mater.*, 2025, **75**, 104021.
55 K. L. Yu, X. J. Lee, C. H. Ong, W. H. Chen, J. S. Chang, C. S. Lin, P. L. Show and C. T. Ling, *Environ. Pollut.*, 2020, **272**, 115986.
56 Z. P. Liu, J. Zhang, L. P. Zhang, Y. Guan, H. Ji, Y. Zhang and H. Gao, *Bioresour. Technol.*, 2023, **376**, 128912.
57 S. Boddu, M. Chavali, J. B. Dulla, V. N. Allugunulla, I. Mikkili, S. Malladi, S. Mannepalli and A. A. Khan, *Biomass Convers. Biorefin.*, 2024, **15**, 15399–15415.
58 J. Y. Kim, H. B. Kim, D. Kwon, Y. F. Tsang, I. H. Nam and E. E. Kwon, *Environ. Res.*, 2024, **262**, 119987.
59 S. Saghir, C. K. Pu, E. F. Fu, Y. Q. Wang and Z. G. Xiao, *Surf. Interfaces*, 2024, **34**, 102357.
60 M. Gao, W. K. Wang, Y. M. Zheng, Q. B. Zhao and H. Q. Yu, *Chem. Eng. J.*, 2020, **402**, 126171.
61 J. M. Davidraj, C. I. Sathish, A. M. Ruban, V. Perumalsamy, V. Narayanan, X. J. Yu, M. B. H. Breese, J. B. Yi and A. Vinu, *Carbon*, 2025, **242**, 120409.
62 P. Saramolee, N. Hwangsud, K. Seneesrisakul, C. Treesatayapun, W. Redpradit, W. Naewrittikul, T. Chaisuwan, J. Johns and U. Thubsuang, *Chem. Eng. J.*, 2025, **503**, 158231.
63 M. Z. Zhong, M. Zhang and X. F. Li, *Carbon Energy*, 2022, **4**, 950–985.
64 Q. Wang, Y. X. Qu, J. Bai, Z. Y. Chen, Q. T. Luo, H. J. Li, J. Li and W. Q. Yang, *Nano Energy*, 2023, **4**, 219–248.
65 S. A. Ansari, N. Parveen, M. Z. Ansari, G. M. Alsulaim, M. W. Alam, M. Y. Khan, A. Umar, I. Hussain and K. L. Zhang, *Prog. Mater. Sci.*, 2025, **154**, 101493.
66 S. Rawat, J. L. Luo, A. A. Ambalkar, S. Hotha, A. Muto and T. Bhaskar, *J. Energy Storage*, 2023, **60**, 106598.
67 Y. Ding, T. Wang, D. Dong and Y. S. Zhang, *Front. Energy Res.*, 2019, **7**, 159.
68 J. S. Tian, T. Zhang, D. Talifu, A. Abulizi and Y. J. Ji, *Mater. Res. Bull.*, 2021, **143**, 111457.
69 M. L. Huang, B. Dai, J. T. Shi, J. Y. Li and C. L. Xia, *Forests*, 2024, **15**, 177.
70 L. Y. Qin, Z. W. Hou, S. Lu, S. Liu, Z. Y. Liu and E. C. Jiang, *Int. J. Electrochem. Sci.*, 2019, **14**, 8907–8918.
71 J. K. Ye, Q. S. Fu, A. Ye, C. K. L. Xu, F. Y. Zhou, X. D. Chen, W. L. Zhu and J. Chen, *Ionics*, 2024, **30**, 1677–1690.
72 E. Adhamash, R. Pathak, Q. Q. Qiao, Y. Zhou and R. M. Taggart, *RSC Adv.*, 2020, **10**, 29910.
73 Y. Gunasekaran, S. Bashir, B. Vengadaesvaran, S. Gunasegeran, T. Zahra, S. Ramesh and K. Ramesh, *Ionics*, 2025, DOI: 10.1007/s11581-025-06334-w.
74 R. Justinabraham, S. Sowmya, A. Durairaj, R. J. Wesley, V. Vijaikanth, A. Obadiah and S. Vasanthkumar, *J. Mater. Sci.*, 2023, **58**, 8445–8462.
75 G. N. Wang, M. J. Guan, R. Fu, C. Yong, Y. Zhu and L. C. Pan, *Diamond Relat. Mater.*, 2024, **143**, 110871.
76 Z. Hu, H. Peng, J. Y. Liu, H. Y. Zhang, S. F. Li, H. L. Wang, Z. Y. Lv, Y. M. Wang, D. Sun, J. F. Tang, L. C. Peng and Y. T. Wang, *Ind. Crops Prod.*, 2023, **202**, 77044.
77 S. Lu, L. Sun, Y. Wang, H. Peng, B. He, X. Yuan, Y. Wang, T. Xia, L. Peng and P. Liu, *Renewable Energy*, 2026, **256**, 124651.